Integrated receiver deghosting and closed-loop surface-multiple elimination

Vrolijk, Jan Willem; Verschuur, Eric; Lopez Angarita, G.A.

DOI
10.1190/GEO2016-0442.1

Publication date
2017

Document Version
Final published version

Published in
Geophysics

GEOPHYSICS, VOL. 82, NO. 4 (JULY-AUGUST 2017); P. T133–T141, 9 FIGS.
10.1190/GEO2016-0442.1

Integrated receiver deghosting and closed-loop surface-multiple elimination

Jan-Willem Vrolijk[1], Eric Verschuur[1], and Gabriel Lopez[1]

ABSTRACT

Accurate surface-related multiple removal is an important step in conventional seismic processing, and more recently, primaries and surface multiples are separated such that each of them is available for imaging algorithms. Current developments in the field of surface-multiple removal aim at estimating primaries in a large-scale inversion process. Using such a so-called closed-loop process, in each iteration primaries and surface multiples will be updated until they fit the measured data. The advantage of redefining surface-multiple removal as a closed-loop process is that certain preprocessing steps can be included, which can lead to an improved multiple removal. In principle, the surface-related multiple elimination process requires deghosted data as input; thus, the source and receiver ghost must be removed. We have focused on the receiver ghost effect and assume that the source is towed close to the sea surface, such that the source ghost effect is well-represented by a dipole source. The receiver ghost effect is integrated within the closed-loop primary estimation process. Thus, primaries are directly estimated without the receiver ghost effect. After receiver deghosting, the upgoing wavefield is defined at zero depth, which is the surface. We have successfully validated our method on a 2D simulated data and on a 2D subset from 3D broadband field data with a slanted cable.

INTRODUCTION

For many marine data sets, accurate removal of surface multiples remains a nontrivial process, especially with a focus on modern broadband data with possible slanted streamers. To properly eliminate surface multiples, it is necessary that the input data are source and receiver deghosted. Dual streamers (Monk, 1990) and multicomponent streamers (Tenghamn et al., 2007; Caprioli et al., 2012) are hardware solutions at the receiver side. In the case of conventional streamers, deghosting is still a challenging preprocessing step. In general, the receiver ghost notch appears inside the desired frequency spectrum in current acquisition techniques that aim at broadband data. Consequently, ghost effects are removed in a separate preprocessing step to improve the image resolution significantly. At the receiver side, Amundsen et al. (2013) describe deghosting as a spatial deconvolution in the frequency domain. To remove the receiver ghost, Ferber et al. (2013) combine pressure data with an estimate of the particle velocity data. Beasley et al. (2013) and Robertsson et al. (2014) use the fact that the upcoming waves arrive earlier than the downgoing ghost waves, leading to causal deghosting filters. Ferber and Beasley (2014) use this principle to shift the ghost events out of the time window. In practice, uncertainties in the estimated water velocity, receiver depth, and a rough sea can lead to errors in the ghost model. To handle these uncertainties, Rickett et al. (2014) and King and Poole (2015) propose adaptive deghosting algorithms that take into account small deviations in these parameters. Grion et al. (2015) describe a method to maximize the kurtosis of the autocorrelation function, to determine which parameters give the best deghosting result. In this paper, the source is assumed to be towed close to the sea surface, such that the source ghost effect is well-represented by a dipole effect. Due to nonlinear effects at the source side and coarse sampling, source deghosting requires a different approach. These limitations on the source side make it a more complex problem compared with the receiver side. Therefore, at the source side, the number of methods is limited for conventional seismic. Some examples are the work of Mayhan and Weglein (2013) and Amundsen and Zhou (2013). In addition, Berkhout and Blacquière (2016) introduce source deghosting as a special case of deblending.

In this paper, removing the receiver ghost is integrated with surface-multiple removal. After receiver deghosting, wavefields that are measured at the receiver depth are now estimated as upgoing wavefields at a zero depth. If one of the earlier receiver deghosting methods is not accurate, this can result in an inaccurate estimate of

Manuscript received by the Editor 19 August 2016; revised manuscript received 2 December 2016; published online 12 April 2017.
[1]Delft University of Technology, Delft, The Netherlands. E-mail: j.w.vrolijk@tudelft.nl; d.j.verschuur@tudelft.nl; g.a.lopezangarita@tudelft.nl.

surface multiples. The surface-related multiple elimination (SRME) method (see amongst others Berkhout, 1982; Verschuur et al., 1992; Berkhout and Verschuur, 1997) has become one of the standard multiple removal tools because it can predict multiples without any knowledge on the subsurface. The theory of SRME uses the estimate of the primary data to predict the surface multiples. This estimated primary data set should ideally have a spike wavelet and no ghost effects. However, usually the wavelet effects are kept in, yielding predicted multiples that exhibit a wrong wavelet, which needs to be corrected for in adaptive subtraction. The latter is usually based on a minimum energy criterion, which is known for not always being optimal for SRME (Nekut and Verschuur, 1998; Guitton and Verschuur, 2004; Aaron et al., 2008; Dragoset et al., 2008).

Therefore, a new approach to multiple removal was developed by van Groenestijn and Verschuur (2009a): estimation of primaries by sparse inversion (EPSI). The main difference with SRME is that prediction and adaptive subtraction are replaced by an inversion process: The primary reflection events are the unknowns in this algorithm and are parameterized in a suitable way. The primaries are estimated such that — together with the associated surface multiples — they explain the input data. In van Groenestijn and Verschuur (2009a), the adopted parameterization consists of band-limited spikes and an effective source wavelet. Examples on complex synthetic and field data sets are shown by van Groenestijn and Verschuur (2009b) and Savels et al. (2011). Baardman et al. (2010) discuss a refinement for dispersion effects, and Lin and Herrmann (2013) develop so-called robust EPSI, which is an implementation that is more robust in terms of optimization and is guaranteed to converge to a global minimum.

Recently, another implementation of the inversion scheme was introduced by Lopez and Verschuur (2015). Their so-called closed-loop SRME (CL-SRME) scheme directly estimates the observed primaries — including the wavelet — and the inverse source operator instead of the band-limited spikes and effective source wavelet in EPSI.

One advantage of writing primary estimation as an inversion problem is the fact that imperfections in the data, which usually have a distorting effect on the SRME output, within EPSI/CL-SRME may be mitigated during the inversion process, if properly handled. This was already shown by van Groenestijn and Verschuur (2009a) and Lopez and Verschuur (2015) for the missing near-offset data. In addition, ghost effects need to be accounted for in SRME-type multiple predictions (Weglein et al., 1997). Therefore, we will need to include the ghost effect in the CL-SRME formalism, such that we are directly estimating the observed primaries including the wavelet without the ghost influence. An initial version to include the ghost in EPSI was already described by Verschuur (2014). However, including the ghost in EPSI results in extrapolation artifacts due to the combination of applying the ghost operator and thresholding in the updating scheme. Including the ghost in CL-SRME can give smaller artifacts that can be handled with the inversion process, as we will show. Another disadvantage of including the ghost in the EPSI approach, as proposed by Verschuur (2014), is that the ghost operator and the inverse ghost operator were assumed to be canceled in the involved multiple prediction step. In case of a slanted cable, this assumption is no longer valid. In CL-SRME, it is possible to estimate the inverse ghost operator together with the inverse source wavelet and leave the ghost operator within the multiple prediction formulation. In the following sections, the theoretical framework of SRME and CL-SRME is described. After that, including the receiver ghost in CL-SRME is explained for a flat streamer and a depth-varying streamer. This method is applied to the 2D synthetic examples and to a 2D field case.

SRME AND CL-SRME: A REVIEW

In Berkhout and Verschuur (1997), it has been proposed to rewrite the surface-related multiple removal scheme of Verschuur et al. (1992) as an iterative procedure:

$$\mathbf{P}_0^{(i+1)} = \mathbf{P} - \mathbf{P}_0^{(i)}\mathbf{A}^{(i)}\mathbf{P}, \tag{1}$$

where $\mathbf{P}_0^{(i)}$ represents the prestack data containing the estimated primaries and the internal multiples in iteration i, $\mathbf{P}$ being the total data (primaries, internal multiples, and surface multiples), and $\mathbf{A}$ representing the so-called surface operator:

$$\mathbf{A} = \mathbf{S}^{-1}\mathbf{R}^{\cap}\mathbf{D}_m^{-1}, \tag{2}$$

where the inverse source $\mathbf{S}^{-1}$ and the receiver properties $\mathbf{D}_m^{-1}$ are combined with the reflectivity at the free surface $\mathbf{R}^{\cap}$. The notation is taken from Berkhout (1982). Note that in our formulation, it is assumed that the data $\mathbf{P}$ have no receiver ghost effects, exhibit a dipole source, and represent upgoing wavefields at the receivers. If the source is towed not too deep, which is often the case, e.g., in our field data example, the source ghost effect may well-represent this dipole effect. Otherwise, proper source deghosting needs to be applied and a so-called obliquity factor needs to be included in the A-operator (see Weglein et al., 1997). Neglecting the obliquity factor will lead to inaccurate prediction of surface multiples in terms of amplitude and phase (Weglein et al., 2003). In practice, accurate source deghosting is limited by coarse sampling in the source direction. To apply source deghosting in a similar way as on the receiver side, the data have to be reconstructed to a dense source sampling.

Each column of a data matrix, e.g., $\mathbf{P}$, contains a wavefield (or a shot record) for one frequency. The primary data $\mathbf{P}_0$ can be written as the source matrix times the primary impulse response matrix:

$$\mathbf{P}_0 = \mathbf{X}_0\mathbf{S}. \tag{3}$$

Each column of the source matrix contains the effective downgoing wavefield for one shot record. In practice, the directivity effects are often neglected or taken into account in a separate preprocessing step (a deghosting process), such that matrix $\mathbf{A}$ can be written as a frequency-dependent scalar $A(\omega)$ (Verschuur and Berkhout, 1997). Thus, the prediction and subsequent adaptive subtraction of the surface-related multiples can be written as

$$\hat{\mathbf{M}}^{(i+1)} = \mathbf{P}_0^{(i)}A^{(i+1)}(\omega)\mathbf{P}; \quad \mathbf{P}_0^{(i+1)} = \mathbf{P} - \hat{\mathbf{M}}^{(i+1)}, \tag{4}$$

where the second step usually assumes minimum energy in the output $\mathbf{P}_0$.

It has been demonstrated that the subtraction of predicted multiples is the weak link in the SRME process because it allows multiples to locally match with strong primary energy, yielding distortions of the primaries and, as a consequence, leaving the residual multiple energy behind (see e.g., Nekut and Verschuur, 1998; Guitton and Verschuur, 2004; Abma et al., 2005). Therefore, in the

CL-SRME algorithm, this subtraction process is avoided by making the primaries the unknowns in a large-scale inversion process.

To describe the CL-SRME algorithm (Lopez and Verschuur, 2015), we again consider equation 1. Through full-waveform inversion, we try to estimate the unknown, multidimensional primaries $\mathbf{P}_0$ and surface operator $\mathbf{A} = \mathbf{S}^{-1}\mathbf{R}^{\cap}\mathbf{D}_m^{-1}$ such that the primaries, including the internal multiples $\mathbf{P}_0$ together with the surface multiples $\mathbf{P}_0\mathbf{AP}$ can explain the total upgoing data $\mathbf{P}$. The difference between the total upgoing data $\mathbf{P}$ and the estimated primaries, including internal multiples plus surface multiples $\hat{\mathbf{P}}_0 + \hat{\mathbf{P}}_0\hat{\mathbf{A}}\mathbf{P}$, is the residual, where the $\hat{}$ indicates an estimated value. The CL-SRME algorithm drives this residual to zero; i.e., it is minimizing the following objective function (see Lopez and Verschuur, 2015):

$$J = \sum_{\omega} \|\mathbf{P} - \hat{\mathbf{P}}_0 - \hat{\mathbf{P}}_0\hat{\mathbf{A}}\mathbf{P}\|^2 + \lambda \sum_{t} \|\hat{\mathbf{p}}_0\|_S, \tag{5}$$

where we usually assume that the surface reflection matrix $\mathbf{R}^{\cap} = -\mathbf{I}$, each data matrix contain one frequency component ω, and t is representing a time slice. In equation 5, $\hat{\mathbf{P}}_0$ and $\hat{\mathbf{A}}$ represent the estimate of the primary data and the estimate of the surface operator that contains the inverse source wavelet, respectively. However, solving the first term of the objective function gives a nonunique solution for $\hat{\mathbf{P}}_0$ and $\hat{\mathbf{A}}$. Therefore, a sparsity-promoting regularization norm $\|\hat{\mathbf{p}}_0\|_S$ is added, where $\hat{\mathbf{p}}_0$ is representing the primaries in the time domain. This can be steered by a user-defined regularization constant. In practice, the total amplitude of the second term is in the order of 1% of the first term. The data residual can be used as a quality control for this constant, if λ is too high, primary energy will leak into the data residual, and it is no longer estimated by the method. To have a better control on the sparsity constraint, a linear Radon transform can be included in the algorithm, such that $\hat{\mathbf{p}}_0$ is assumed to be sparse in the linear Radon domain. In the field data example, using the linear Radon domain gave a significant uplift for the result, but in the synthetic case, there was no significant difference in the result of the estimated primaries.

INCLUDING THE RECEIVER GHOST IN CL-SRME

When the receiver ghost effect is included in CL-SRME, the forward model for equation 1 becomes

$$\mathbf{P}_g = \mathbf{D}_g\mathbf{P}_0 + \mathbf{D}_g\mathbf{P}_0\mathbf{A}\mathbf{D}_g^{-1}\mathbf{P}_g, \tag{6}$$

where the detector operator $\mathbf{D}_g$ contains the ghost effect at the receiver side and $\mathbf{P}_g$ represents the measured data including the detector ghost. The total detector operator becomes $\mathbf{D} = \mathbf{D}_m\mathbf{D}_g$. Each column in matrix $\mathbf{D}_g$ contains the effective operator that modifies the upgoing wavefield at the surface z_0 to the receiver level, being defined as

$$\mathbf{D}_g(z_d, z_0) = \mathbf{F}(z_d, z_0) + \mathbf{W}(z_d, z_0)\mathbf{R}^{\cap}, \tag{7}$$

where $\mathbf{W}(z_d, z_0)$ describes the forward propagation from the surface — after reflection — toward the detector level z_d and $\mathbf{F}(z_d, z_0) \approx [\mathbf{W}(z_d, z_0)]^{\mathrm{H}}$ describes an inverse propagation from the surface to the detector level, where superscript H indicates the Hermitian, i.e., the complex conjugate of the transposed matrix. In the case in which the receiver cable is flat, each column $\mathbf{D}_g(z_d, z_0)$ can be calculated as the inverse spatial Fourier transform of the wavenumber operator:

$$\tilde{D}_g(k_x; \omega) = e^{+jk_z\Delta z} + R^{\cap}e^{-jk_z\Delta z}, \tag{8}$$

with k_z being the vertical wavenumber ($k_z = \sqrt{(k^2 - k_x^2)}$, with horizontal wavenumber k_x, wavenumber $k = \omega/c$, c being the propagation velocity in water, and $\Delta z = |z_0 - z_d|$. If we assume the flat cable situation, we can see in the last term of equation 6 that we first remove the ghost effect from the measurements $\mathbf{P}_g$, creating the upgoing wavefield at the surface, after which it is convolved with operator $\mathbf{A}$ and the primaries $\mathbf{P}_0$ to predict the multiples. Finally, the ghost effect has to be included in the predicted multiples to match it with the observed data. However, assuming that the subsurface structures are moderate, such that the arrival angles of the events do not change much from source to receiver side, these two ghost response matrices approximately cancel, which can be the case for a flat cable configuration:

$$\mathbf{P}_g \approx \mathbf{D}_g\mathbf{P}_0 + \mathbf{P}_0\mathbf{A}\mathbf{P}_g. \tag{9}$$

If the cable is slanted, then the operator $\mathbf{D}_g$ — strictly speaking — cannot be used anymore in our matrix notation because every receiver position has a different depth. Therefore, an operator table is constructed containing matrices $\mathbf{D}_g$ for each receiver depth. For each shot record, i.e., column of the data matrix $\mathbf{P}$, a ghost operator $\mathbf{D}_{g,j}$ is constructed from this operator table that takes into account the different receiver depths. This approximation only holds if there are small depth changes between consecutive receivers. In fact, equation 6 should be written separately for each shot record with corresponding ghost operator because the receiver depths can vary for each shot:

$$\mathbf{P}_g = \mathbf{P}_{g_0} + \mathbf{P}_{g_0}\hat{\mathbf{A}}\mathbf{P}_{dg}, \tag{10}$$

where

$$\mathbf{P}_{g_0} = \{\mathbf{D}_{g,1}\hat{\mathbf{P}}_{0,1}; \ldots; \mathbf{D}_{g,j}\hat{\mathbf{P}}_{0,j}; \ldots; \mathbf{D}_{g,N}\hat{\mathbf{P}}_{0,N}\}, \tag{11}$$

and

$$\mathbf{P}_{dg} = \{\mathbf{D}_{g,1}^{-1}\mathbf{P}_{g,1}; \ldots; \mathbf{D}_{g,j}^{-1}\mathbf{P}_{g,j}; \ldots; \mathbf{D}_{g,N}^{-1}\mathbf{P}_{g,N}\}, \tag{12}$$

where $\mathbf{P}_{g_0}$ is the primaries including the ghost operator and $\mathbf{P}_{dg}$ is the measured data including the ghost effect convolved with the inverse ghost operator. Thus, for each specific shot record j for a data set with a total of N shots, the primary data $\hat{\mathbf{P}}_{0,j}$ are convolved with the corresponding ghost operator $\mathbf{D}_{g,j}$ and the measured data $\hat{\mathbf{P}}_{g,j}$ are convolved with the corresponding inverse ghost operator $\mathbf{D}_{g,j}^{-1}$. In this case, the arrival angles of the events do change from source to receiver side and the approximations do not hold anymore. Therefore, $\mathbf{D}_{g,j}^{-1}$ will be estimated from the ghost operator $\mathbf{D}_{g,j}$ using a stabilized matrix inversion for each frequency:

$$\mathbf{D}_{g,j}^{-1} \approx \mathbf{D}_{g,j}^{\mathrm{H}}[\mathbf{D}_{g,j}^{\mathrm{H}}\mathbf{D}_{g,j} + \epsilon\mathbf{I}]^{-1}, \tag{13}$$

where ϵ is some stabilization value and $\mathbf{I}$ is the identity matrix.

Knowing the receiver depths, even for a slanted cable, the ghost operator is deterministic and can easily be included in the CL-SRME algorithm.

Based on the forward models in equation 9 or 10, now two new objective functions can be determined for a flat and a slanted configuration that should be minimized, meaning driving the residual data to zero. We will use

$$J = \sum_{\omega} \|\mathbf{P}_g - \mathbf{D}_g\hat{\mathbf{P}}_0 - \hat{\mathbf{P}}_0\hat{\mathbf{A}}\mathbf{P}_g\|^2 + \lambda \sum_{t} \|\hat{\mathbf{p}}_0\|_S, \quad (14a)$$

for the horizontal cable and

$$J = \sum_{\omega} \|\mathbf{P}_g - \mathbf{P}_{g_0} - \mathbf{P}_{g_0}\hat{\mathbf{A}}\mathbf{P}_{dg}\|^2 + \lambda \sum_{t} \|\hat{\mathbf{p}}_0\|_S, \quad (14b)$$

for the slanted cable. This means that to evaluate an obtained estimate of the (ghost-free) primaries $\hat{\mathbf{P}}_0$, a forward ghosting process needs to be involved to compare the estimated (ghost-free) primaries and the estimated (ghost-free) multiples in case of the slanted cable with the observed data that include a ghost. Next, the gradients of the objective functions with respect to the primary data need to be determined, which read

$$\Delta\mathbf{P}_0^{(i)} = 2\{\mathbf{D}_g^{\mathrm{H}}\mathbf{V}^{(i)} + \mathbf{V}^{(i)}[\mathbf{A}\mathbf{P}_g]^{\mathrm{H}}\} + \lambda \cdot \mathrm{sgn}(\hat{\mathbf{p}}_0) \quad (15a)$$

and

$$\Delta\mathbf{P}_{0,j}^{(i)} = 2\mathbf{D}_{g,j}^{\mathrm{H}}\{V_j^{(i)} + (\mathbf{V}^{(i)}[\mathbf{A}\mathbf{P}_{dg}]^{\mathrm{H}})_j\} + \lambda \cdot \mathrm{sgn}(\hat{\mathbf{p}}_0), \quad (15b)$$

where $\mathbf{V}$ indicates the residual data in the case of data with a ghost and the gradient of the sparsity promoting term is expressed by the signum function. Note that in the calculation of the update for $\mathbf{P}_0$ or $\mathbf{P}_{0,j}$ now also one or two adjoint ghosting operators are involved. This adjoint ghost operator makes sure that the contribution to the primaries in the data gets a ghost-free character, as is expected for the primaries.

Besides these modifications to the forward model, the objective function and the gradient, the CL-SRME algorithm remains largely the same, as described by Lopez and Verschuur (2015).

MODELED DATA

We will demonstrate the effect of ghosts on CL-SRME for a flat and slanted cable. The data are modeled with an acoustic finite-difference scheme. The three-reflector velocity model with a reflecting bottom boundary for this scheme is illustrated in Figure 1. The source and receiver sampling is 15 m. Extended CL-SRME is applied to a fixed-spread configuration of 401 sources × 401 receivers with a sampling of 4 ms.

In the first case, the data are modeled with a cable at 25 m depth. A single shot from these data is illustrated in Figure 2a. To validate the results after CL-SRME, a data set is also modeled without the receiver ghost effect, and thus with a cable at zero depth (Figure 2b).

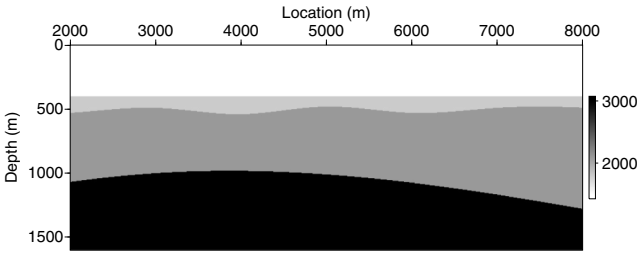

Figure 1. Velocity model for the acoustic finite-difference modeling scheme. Note that the bottom also acts as a reflector.

For better comparison, both of these data sets are modeled with a source ghost at 5 m depth, which gives the data a dipole source character. To obtain Figure 2c, the inverse ghost operator from equation 13, calculated via stabilized least-squares inversion, is applied to the input shot (Figure 2a) and followed by CL-SRME. After this cascaded approach, most of the surface-multiple energy is removed. However, compared with the reference shot (Figure 2a), some surface-multiple energy leaked into the domain of primaries, i.e., around the third event and below the bottom reflection. The ringing events above the bottom reflection already indicate that receiver deghosting was not accurate, and the results in the frequency domain confirm this (Figure 3a–3c). In the frequency domain, the notch effect of the ghost is visible at 30 Hz (Figure 3a), which corresponds to the cable depth of 25 m. In Figure 3c, there is still a clear imprint from the ghost notch that is supposed to be completely filled in (Figure 3b). In Figure 4a–4c, the input stacked section is compared with the stacked section of the reference primary data and with the stacked section after consecutive deghosting and CL-SRME. Again, it is visible that the surface-multiple energy leaked into the primary data domain after the cascaded approach.

The result for a single shot from CL-SRME including the receiver ghost is illustrated in Figure 2d. The primaries are estimated more accurately compared with the cascaded result (Figure 2c), and the

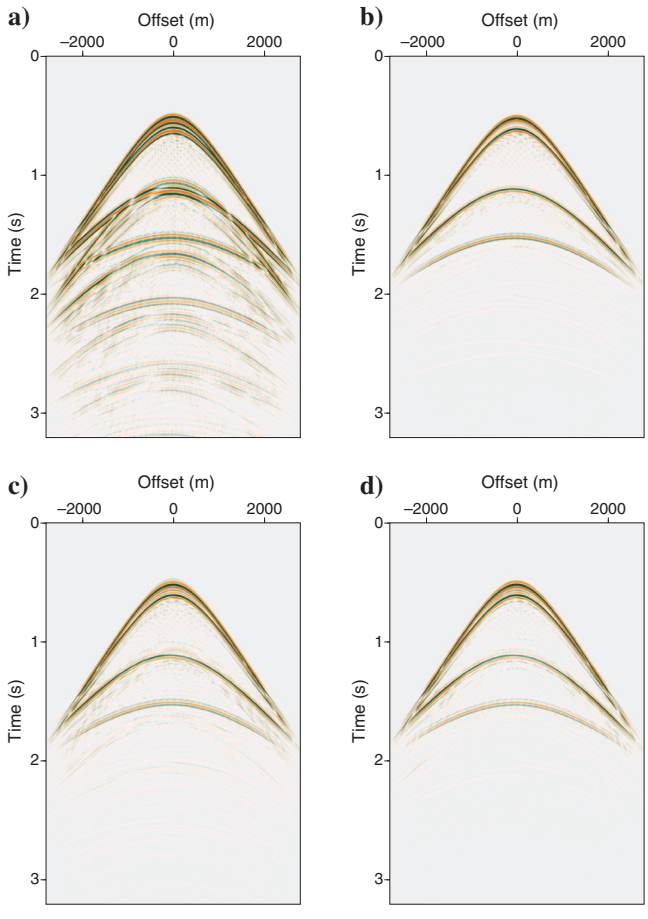

Figure 2. Results for a shot from the synthetic data with a 25 m receiver ghost effect. (a) Input shot including the ghost. (b) Modeled primaries. (c) Primaries after deghosting followed by CL-SRME. (d) Primaries after CL-SRME including the ghost.

sidelobes of the ghost events are better focused to a single event. The remaining surface-multiple energy around the third reflector and below the bottom reflector is better suppressed. However, there is sill some multiple energy visible. These events are also visible in the reference shot (Figure 2a); thus, they must be related to internal multiples. Only around offset, 2000 m, below the bottom event, is some surface-multiple energy still present. After including the receiver ghost in CL-SRME, the notch effect is completely filled in (Figure 3d). Although there is some discrepancy for the amplitudes in the notch area, this result is significantly better than the cascaded case (Figure 3c). The same holds for the lower frequency area: Figure 3d shows an improved reconstruction of the information down to about 3 Hz compared with Figure 3c. At less than 3 Hz, we see some inversion artifacts because for that range, the input data (Figure 3a) do not contain information. In Figure 4d, the stacked section after CL-SRME including the receiver ghost is illustrated. Again, a better surface-multiple removal is obtained; however, also internal multiples are a bit suppressed. Probably, relaxing the sparseness constraint can prevent the algorithm from doing this. Thus, including the ghost operator in CL-SRME gave a significant uplift, in the surface-multiple prediction and receiver deghosting, compared with applying a least-squares deghosting followed by CL-SRME.

In the second case, the data are modeled using a slanted cable with a depth varying from 20 to 60 m. The results are illustrated in Figures 5 and 6. The deghosting effect for the slanted cable after including the ghost in CL-SRME is again quite accurate: The primary events that clearly display the slanted-cable ghost effect at the larger offsets (Figure 5a) are focused to one event after deghosting (Figure 5b). In the frequency domain (Figure 5c), the notch effect is visible and due to the slanted cable configuration; it becomes significantly more offset dependent compared with the fixed-depth case (Figure 3a). After extended CL-SRME (Figure 5d), the different order notches are filled in, although compared with the flat cable

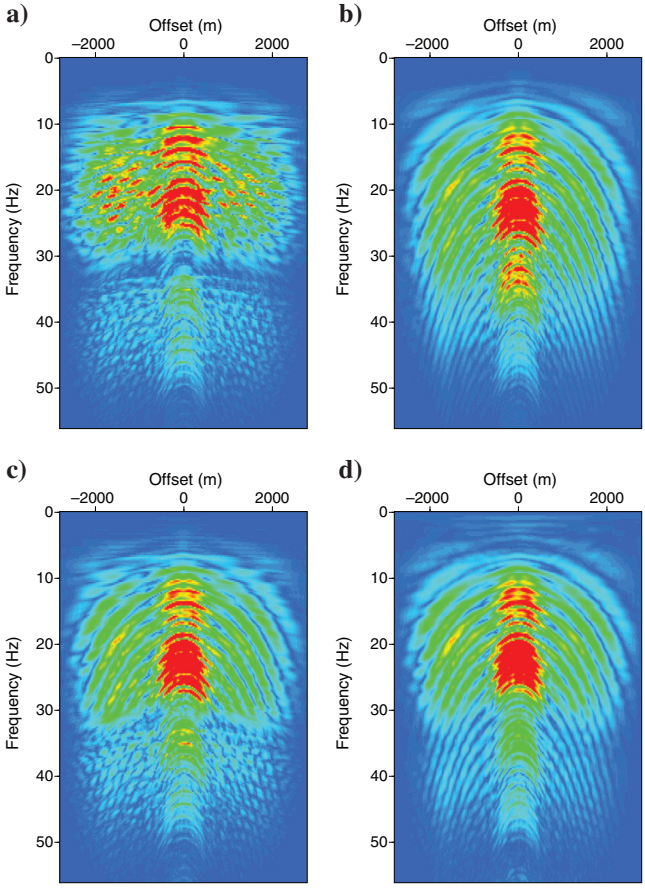

Figure 3. Results for a shot from the synthetic data with a 25 m receiver ghost effect in the frequency domain. (a) Input shot including the ghost. (b) Modeled primaries. (c) Primaries after deghosting followed by CL-SRME. (d) Primaries after CL-SRME including the ghost.

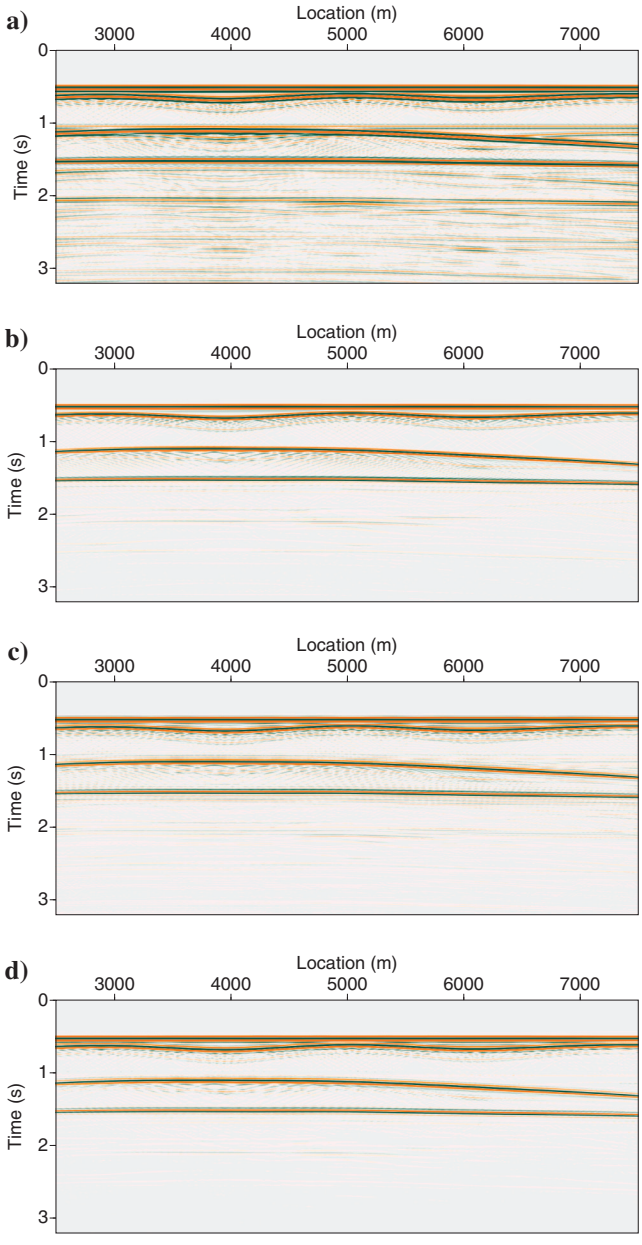

Figure 4. Results from extended CL-SRME for the synthetic data with a 25 m receiver ghost effect. (a) Input stacked section including receiver ghost. (b) Stacked section of modeled primaries. (c) Stacked section of primaries after deghosting followed by CL-SRME. (d) Stacked section of primaries after CL-SRME including the ghost.

configuration, it is more noisy. In addition, more multiple energy leaked into the primary data domain compared with the flat cable situation, especially for larger offsets (see Figure 5b). The input stacked section in Figure 6a is compared with the output stacked section after extended CL-SRME in Figure 6b. Note again that somewhat more multiple energy leaked into the primary domain compared with the flat cable situation. These artifacts may come from the fact that in this method, an approximation for $[\mathbf{D}_j]^{-1}$ is used. Further research is needed to justify whether this is the reason for these artifacts.

BROADBAND FIELD DATA

Finally, we demonstrate the application of CL-SRME including the receiver ghost to a broadband (3–150 Hz) data set from Australia, provided by CGG. CL-SRME is applied with the $\mathbf{D}_j$ operator now describing the effect of a slanted cable with a depth increasing from 8 to 57.5 m. The original source sampling is 37.5 m, and the original receiver sampling is 12.5 m. Reconstruction and near-offset interpolation are applied via a hybrid linear and parabolic Radon domain, respectively (see Verschuur et al., 2012) to obtain a source sampling and receiver sampling of 12.5 m and to fill in the near-offset data. CL-SRME is applied to a subset of 801 shots and receivers of this data set with a sampling of 2 ms. In Figures 7a, 8a, and 9a, the input data for CL-SRME are shown, respectively, in the shot, a magnified shot, and a time-migrated domain. A band-pass filter and f-k filter are applied to the shots for display purposes. After time migration, in addition, the spectrum is whitened. Figures 7b, 8b, and 9b are the ghost-free primaries, thus the outcome of CL-SRME. To delineate the effect of just the multiple removal, the ghost operator was applied to the final ghost-free result, as displayed in Figures 7c, 8c, and 9c. The estimated surface multiples are illustrated in Figures 7d, 8d, and 9d. The deghosting for the slanted cable after CL-SRME is quite accurate: the events at approximately 1.25 and 1.75 s, indicated by the red arrows, that clearly display the slanted-cable ghost effect (Figures 7a, 7b, 8a, and 8b) become focused (Figures 7c and 8c). Also, the phase of the events is corrected by the algorithm. In Figures 7a and 8a, two surface multiples are indicated by the yellow arrows, and after CL-SRME (Figures 7c and 8c), most of the energy related to these surface multiples is removed. Nevertheless, overall in the shots, there is some surface-multiple energy left, so this can indicate that the wavelet is not yet estimated perfectly. The latter could be due to applying a 2D method to data with 3D amplitudes and/or due to an inaccurate near-offset interpolation for this relatively shallow-water data set. On the other hand, if we focus on the time-migrated sections after CL-SRME, most of the multiple energy is suppressed (see, i.e., the yellow arrows indicating multiples in Figure 9a–9c) and the resolution is significantly higher. For example, the red arrows in Figure 9a–9c indicate several events that become visible due to removing the ghost effect.

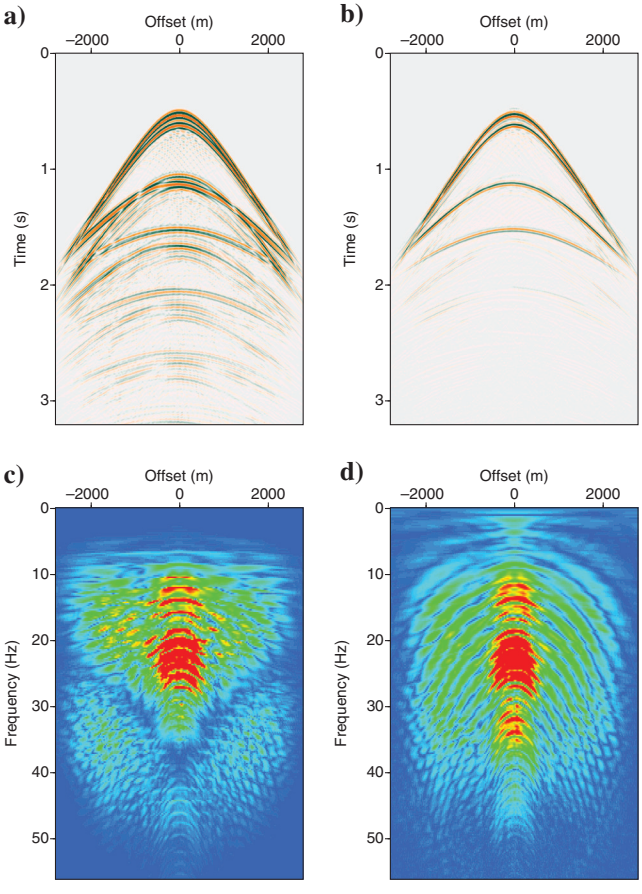

Figure 5. Results from CL-SRME with ghost effect for the input data with a 20–60 m slanted cable. (a) Input shot with ghost. (b) CL-SRME primaries. (c) Input shot in the frequency domain. (d) CL-SRME primaries in the frequency domain.

DISCUSSION

Most of the surface-multiple energy was removed from the field data, although there is some leakage into the primaries that probably can be handled with extending the CL-SRME to the full 3D case. The surface multiples will be matched as well as possible to the input data by the CL-SRME algorithm. However, a 2D approxima-

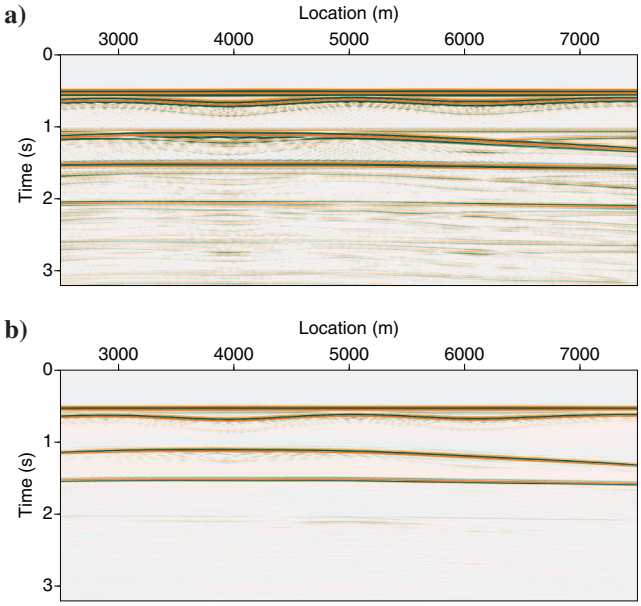

Figure 6. Results from CL-SRME for synthetic data with a 20–60 m slanted cable. (a) Input stacked section with ghost. (b) Stacked section of CL-SRME primaries.

tion of wavefield propagation will never accurately explain wavefields that are 3D in practice. Especially, if there are dips present in the crossline direction, which is very likely for this field data set, another cause for this surface-multiple leakage can be due to the limitations of near-offset interpolation for shallow reflectors. Lopez and Verschuur (2015) describe that it is possible to combine near-offset interpolation with CL-SRME by implementing the scheme in the focal domain. This approach will probably result in more accurate near offsets and surface multiples.

In a rough and or varying sea, $\mathbf{R}$ is not equal to $-\mathbf{I}$, especially for higher frequencies (Orji et al., 2013). In practice, a wrong $\mathbf{R}$ will result in ringing events and to some extent, due to the L1-norm, the algorithm still would be able to suppress these effects. However, the algorithm can be helped by putting more a priori knowledge of $\mathbf{R}$ in, if available. Another problem in practice is that exact knowledge of receiver locations is not available; there is always some uncertainty, and even a flat cable will have some depth variations along the streamer. This will result in a mismatch between estimated ghost and input data; however, to some extent, again due to the L1-norm, the algorithm still would be able to suppress these effects. Another way to handle these uncertainties can be estimating the ghost operator adaptively during the CL-SRME process. Further research is necessary to investigate these uncertainties and their solutions more thoroughly.

An alternative to the method proposed in this paper is to apply a more sophisticated receiver deghosting and CL-SRME in a cascaded manner. A dedicated deghosting algorithm can be implemented in a closed-loop manner without the surface-multiple prediction. Recently, Rickett et al. (2014) and King and Poole (2015) show results in which such a closed-loop deghosting process is applied in the local plane-wave domain and can adapt to small errors in the propagation operator. In Wang et al. (2014), a similar method is combined with interpolation in the crossline direction to make it applicable to 3D data with coarse sampling in one direction. Berkhout and Blacquière (2016) show a closed-loop approach based on a nonlinear deblending algorithm. In this paper, we could only demonstrate the limitations of a standard deghosting procedure followed by CL-SRME. Further research is necessary to conclude if deghosting combined with multiple removal is more accurate and/or more efficient than an approach in which a dedicated, advanced deghosting procedure is followed by CL-SRME.

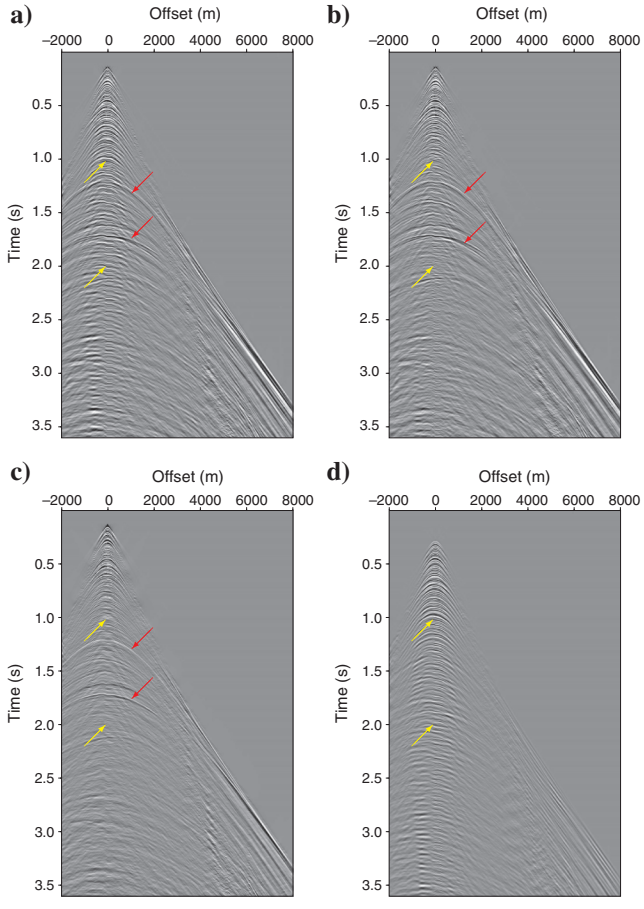

Figure 7. Results from CL-SRME for the field data with a slanted cable. The red arrows indicate receiver ghost effects, and the yellow arrows indicate surface multiples. (a) Input shot with the ghost effect and surface multiples. (b) CL-SRME primaries with the ghost effect. (c) CL-SRME primaries without the ghost effect. (d) CL-SRME surface multiples.

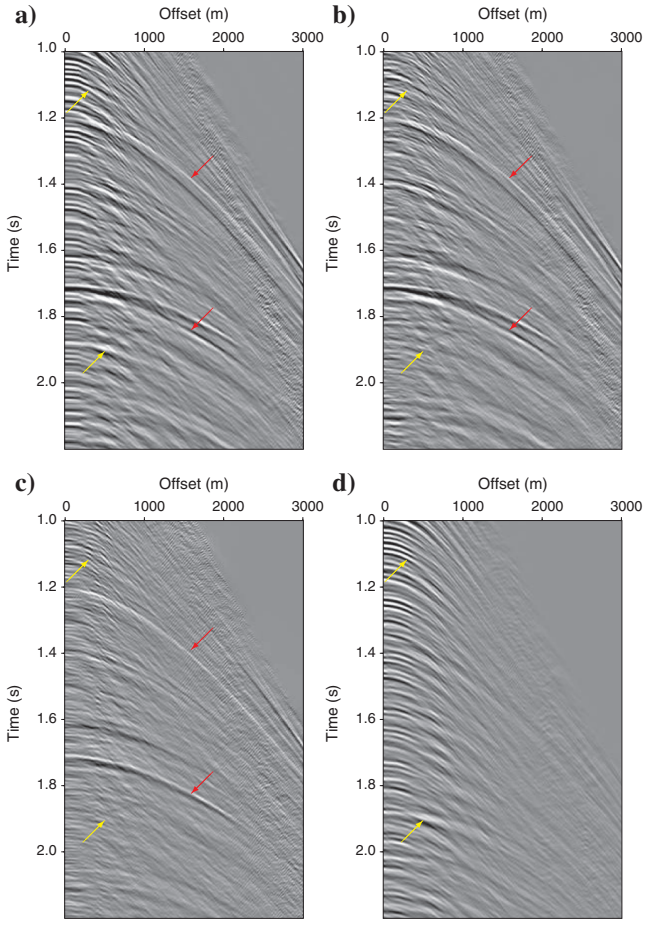

Figure 8. Magnified pictures from Figure 7. The red arrows indicate receiver ghost effects, and the yellow arrows indicate surface multiples. (a) Input shot with the ghost effect and surface multiples. (b) CL-SRME primaries with the ghost effect. (c) CL-SRME primaries without the ghost effect. (d) CL-SRME surface multiples.

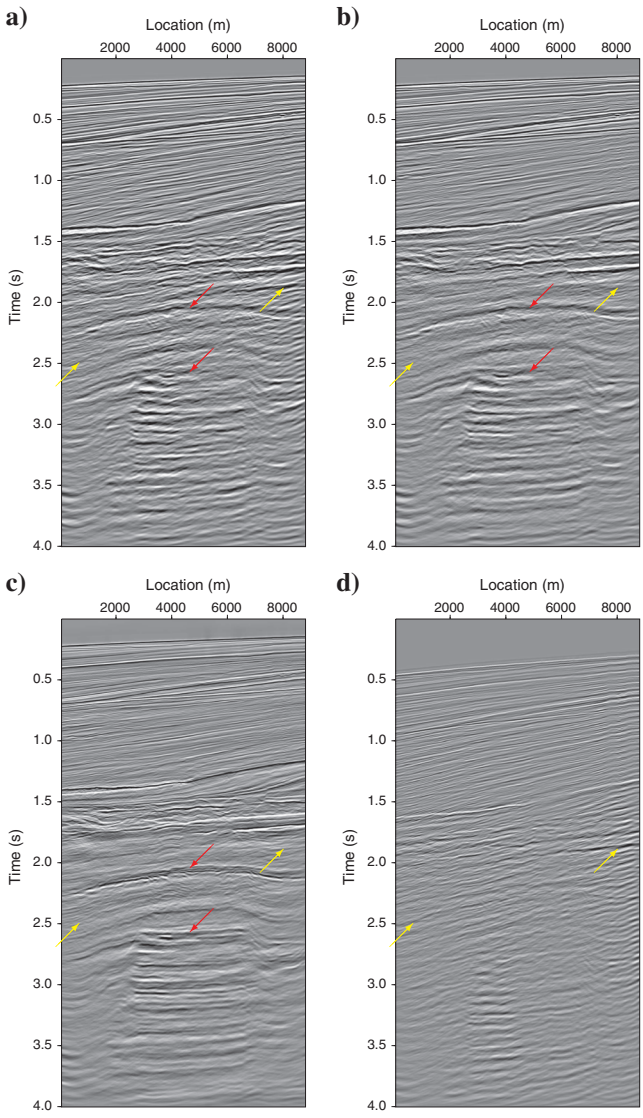

Figure 9. Results from CL-SRME for the field data with a slanted-cable ghost effect after time migration. The red arrows indicate receiver ghost effects, and the yellow arrows indicate surface multiples. (a) Input time-migrated section with the ghost effect and surface multiples. (b) CL-SRME time-migrated section for primaries with the ghost effect. (c) CL-SRME time-migrated section for primaries without the ghost effect. (d) CL-SRME time-migrated section for the surface multiples.

Note that for our current solution, the extra cost of CL-SRME when including the ghost effect is relatively low compared with standard CL-SRME: It is approximately 10%–15% more expensive in case of a slanted cable.

CONCLUSIONS

We demonstrated that the CL-SRME algorithm can be extended to handle receiver ghost effects. In the slanted cable case, we took into account that it is not valid to cancel out the ghost operators in the multiple prediction term. As a result, we used an approximate inverse ghost operator during the multiple prediction process. The results after CL-SRME including the slanted-cable ghost effect for synthetic and field data are quite accurate. Minor residual surface multiples in the output may be due to using an approximate inverse ghost operator during the prediction. Extending this method to the full 3D case will be necessary to further improve the field data results. Besides, further research is needed to determine whether a cascaded approach of receiver deghosting and CL-SRME is more beneficial than combining both methods in one inversion scheme.

ACKNOWLEDGMENTS

The authors would like to thank CGG for providing the field data set and the sponsors of the Delphi Research Consortium for their support. In addition, they thank the six anonymous reviewers for their valuable comments that have helped to improve this paper.

REFERENCES

Aaron, P., R. O'Toole, S. Barnes, R. F. Hegge, and R. G. van Borselen, 2008, True-azimuth versus zero-azimuth 3-D multiple prediction in WATS processing: 78th Annual International Meeting, SEG, Expanded Abstracts, 2431–2435.

Abma, R. L., M. M. N. Kabir, K. H. Matson, S. Mitchell, S. A. Shaw, and W. McLain, 2005, Comparisons of adaptive subtraction methods for multiple attenuation: The Leading Edge, **24**, 277–280, doi: 10.1190/1.1895312.

Amundsen, L., and H. Zhou, 2013, Low-frequency seismic deghosting: Geophysics, **78**, no. 2, WA15–WA20, doi: 10.1190/geo2012-0276.1.

Amundsen, L., H. Zhou, A. Reitan, and A. B. Weglein, 2013, On seismic deghosting by spatial deconvolution: Geophysics, **78**, no. 6, V267–V271, doi: 10.1190/geo2013-0198.1.

Baardman, R. H., D. J. Verschuur, R. G. van Borselen, M. O. Frijlink, and R. F. Hegge, 2010, Estimation of primaries by sparse inversion using dual sensor data: 80th Annual International Meeting, SEG, Expanded Abstracts, 3468–3472.

Beasley, C. J., R. C. Y. Ji, and J. Perdomo, 2013, Wave equation receiver deghosting: A provocative example: 83rd Annual International Meeting, SEG, Expanded Abstracts, 133–135.

Berkhout, A. J., 1982, Seismic migration, imaging of acoustic energy by wave field extrapolation, part A: Theoretical aspects (2nd ed.): Elsevier.

Berkhout, A. J., and G. Blacquière, 2016, Deghosting by echo-deblending: Geophysical Prospecting, **64**, 406–420, doi: 10.1111/gpr.2016.64.issue-2.

Berkhout, A. J., and D. J. Verschuur, 1997, Estimation of multiple scattering by iterative inversion — Part 1: Theoretical considerations: Geophysics, **62**, 1586–1595, doi: 10.1190/1.1444261.

Caprioli, P., K. Özdemir, A. Özbek, J. Kragh, D. van Manen, P. Christie, and J. Robertsson, 2012, Combination of multi-component streamer pressure and vertical particle velocity — Theory and application to data: 74th Annual International Meeting, EAGE, Extended Abstracts, A033.

Dragoset, W. H., I. Moore, M. Yu, and W. Zhao, 2008, 3D general surface multiple prediction: An algorithm for all surveys: 78th Annual International Meeting, SEG, Expanded Abstracts, 2426–2430.

Ferber, R., and C. J. Beasley, 2014, Simulating ultra-deep-tow marine seismic data for receiver deghosting: 76th Annual International Meeting, EAGE, Extended Abstracts, ELI1.

Ferber, R., P. Caprioli, and L. West, 2013, L1 pseudo-vz estimation and deghosting of single-component marine towed-streamer data: Geophysics, **78**, no. 2, WA21–WA26, doi: 10.1190/geo2012-0293.1.

Grion, S., R. Telling, and J. Barnes, 2015, De-ghosting by kurtosis maximisation in practice: 85th Annual International Meeting, SEG, Expanded Abstracts, 4605–4609, doi: 10.1190/segam2015-5902239.1.

Guitton, A., and D. J. Verschuur, 2004, Adaptive subtraction of multiples using the l1-norm: Geophysical Prospecting, **52**, 27–38, doi: 10.1046/j.1365-2478.2004.00401.x.

King, S., and G. Poole, 2015, Hydrophone-only receiver deghosting using a variable sea surface datum: 85th Annual International Meeting, SEG, Expanded Abstracts, 4610–4614.

Lin, T. Y., and F. J. Herrmann, 2013, Robust estimation of primaries by sparse inversion via one-norm minimization: Geophysics, **78**, no. 3, R133–R150, doi: 10.1190/geo2012-0097.1.

Lopez, A. G., and D. J. Verschuur, 2015, Closed-loop surface-related multiple elimination and its application to simultaneous data reconstruction: Geophysics, **80**, no. 6, V189–V199, doi: 10.1190/geo2015-0287.1.

Mayhan, J. D., and A. B. Weglein, 2013, First application of Green's theorem-derived source and receiver deghosting on deep-water Gulf of Mexico

synthetic SEAM and field data: Geophysics, **78**, no. 2, WA77–WA89, doi: 10.1190/geo2012-0295.1.
Monk, D. J., 1990, Wavefield separation of twin streamer data: First Break, **8**, 96–104, doi: 10.3997/1365-2397.1990007.
Nekut, A. G., and D. J. Verschuur, 1998, Minimum energy adaptive subtraction in surface related multiple elimination: 68th Annual International Meeting, SEG, Expanded Abstracts, 1507–1510.
Orji, O. C., W. Sollner, and L. J. Gelius, 2013, Sea surface reflection coefficient estimation: 83rd Annual International Meeting, SEG, Expanded Abstracts, 2150–2153.
Rickett, J., D.-J. V. Manen, P. Loganathan, and N. Seymour, 2014, Slanted-streamer data adaptive de-ghosting with local plane waves: 76th Annual International Meeting, EAGE, Extended Abstracts, Th ELI 15, doi: 10.3997/2214-4609.20141453.
Robertsson, J. O. A., L. Amundsen, and O. Pedersen, 2014, Deghosting of arbitrarily depth varying marine hydrophone streamer data by time-space domain modelling: 84th Annual International Meeting, SEG, Expanded Abstracts, 4248–4252.
Savels, T., K. de Vos, and J. W. de Maag, 2011, Surface multiple attenuation through sparse inversion: Results for complex synthetics and real data: First Break, **29**, 55–64, doi: 10.3997/1365-2397.2011003.
Tenghamn, R., S. Vaage, and C. Borresen, 2007, A dual sensor towed marine streamer: Its viable implementation and initial results: 77th Annual International Meeting, SEG, Expanded Abstracts, 989–993.
van Groenestijn, G. J. A., and D. J. Verschuur, 2009a, Estimating primaries by sparse inversion and application to near-offset data reconstruction: Geophysics, **74**, no. 3, A23–A28, doi: 10.1190/1.3111115.
van Groenestijn, G. J. A., and D. J. Verschuur, 2009b, Estimation of primaries and near offsets by sparse inversion: Marine data applications: Geophysics, **74**, no. 6, R119–R128, doi: 10.1190/1.3213532.
Verschuur, D. J., 2014, Generalization of the EPSI primary estimation algorithm for deep towed and slanted cables: 76th Annual International Meeting, EAGE, Extended Abstracts, Tu E102 02, doi: 10.3997/2214-4609.20140670.
Verschuur, D. J., and A. J. Berkhout, 1997, Estimation of multiple scattering by iterative inversion — Part 2: Practical aspects and examples: Geophysics, **62**, 1596–1611, doi: 10.1190/1.1444262.
Verschuur, D. J., A. J. Berkhout, and C. P. A. Wapenaar, 1992, Adaptive surface-related multiple elimination: Geophysics, **57**, 1166–1177, doi: 10.1190/1.1443330.
Verschuur, D. J., J. W. Vrolijk, and C. Tsingas, 2012, 4D reconstruction of wide azimuth (WAZ) data using sparse inversion of hybrid radon transforms: 82nd Annual International Meeting, SEG, Expanded Abstracts, doi: 10.1190/segam2012-1098.1.
Wang, P., S. Ray, and K. Nimsaila, 2014, 3D joint deghosting and crossline interpolation for marine single-component streamer data: 84th Annual International Meeting, SEG, Expanded Abstracts, 3594–3598.
Weglein, A. B., F. V. Araujo, P. M. Carbvalho, R. H. Stolt, K. H. Matson, R. T. Coates, D. Corrigan, D. J. Foster, S. A. Shaw, and H. Zhang, 2003, Topical review: Inverse scattering series and seismic exploration: Inverse Problems, **19**, R27–R83, doi: 10.1088/0266-5611/19/6/R01.
Weglein, A. B., F. A. Gasparotto, P. M. Carvalho, and R. H. Stolt, 1997, An inverse scattering series method for attenuating multiples in seismic reflection data: Geophysics, **62**, 1975–1989, doi: 10.1190/1.1444298.